Applied Catalysis B: Environmental 251 (2019) 94–101

Contents lists available at ScienceDirect

Applied Catalysis B: Environmental

journal homepage: www.elsevier.com/locate/apcatb

Photocatalytic hydrogen evolution on P-type tetragonal zircon $BiVO_4$

Junpeng Wang[a,b,*], Yanan Song[a], Jing Hu[c], Yu Li[a], Zeyan Wang[b], Ping Yang[a,**], Gang Wang[a], Qian Ma[a], Quande Che[a], Ying Dai[b], Baibiao Huang[b,**]

[a] School of Material Science and Engineering, University of Jinan, Jinan, 250022, PR China
[b] State Key Laboratory of Crystal Materials, Shandong University, Jinan, 250100, PR China
[c] School of Chemistry and Pharmaceutical Engineering, Qilu University of Technology, Jinan, 250353, PR China

ARTICLE INFO

Keywords:
P-type
Bismuth vanadate
Hot carriers
Photocatalytic
Hydrogen evolution

ABSTRACT

Tetragonal zircon $BiVO_4$ (P-$BiVO_4$) were grown on fluorine-doped tin oxide (FTO) glass via hydrothermal method. The cathodic photocurrent and Mott-Schottky analysis indicate that the tetragonal zircon $BiVO_4$ is a p-type semiconductor. Inductively coupled plasma (ICP) analysis and X-ray photoelectron spectrum showed that there are Bi vacancies and interstitial oxygen exist in the crystal, which are the origin of the p-type conductivity. The flat band potential of the P-$BiVO_4$ is about 1.33 V (vs Ag/AgCl) inferred from Mott-Schottky plots. Combining with diffuse reflection spectrum and valence band X-ray photoelectron spectrum, the calculated conduction band value of the P-$BiVO_4$ is about 0.06 V vs RHE, slightly higher than the reduction potential of hydrogen. However, the P-$BiVO_4$ exhibit hydrogen production activity under Xe light irradiation even though its conduction band level is not negative enough. This can be attributed to the hot carrier processes in p-type semiconductors.

1. Introduction

Catalytic hydrogen production is believed to be critical for the energy and environmental sustainability [1–4]. Solar energy is a most clean, abundant renewable energy source, so photocatalytic water splitting is considered as one of the most promising ways to obtain H2. A series of non-toxic, economically and stable semiconductors such as TiO_2, ZnO, $BiVO_4$ and Fe_2O_3 et al. have been developed and used as photocatalysts for water splitting [5–13]. However, most of such oxide semiconductors are intrinsic n-type for the existence of oxygen vacancies [14]. The surface band bending of n-type semiconductors creates an additional energy barrier which hinder the transmission of photo-generate electrons to semiconductor-solution interfaces, resulting in the low hydrogen production efficiency [15]. P-type semiconductor, by contrast, has a higher water reduction efficiency for its downward band bending when contacted with water. As a result, photocathodes are usually p-type semiconductors.

Compared with the large number of n-type semiconductors, there are only a few reports on p-type photocatalytic materials. In order to obtained p-type semiconductor photocatalyst, great efforts have been made to improve the fabrication technique and exploit new methods. P-type TiO_2, Fe_2O_3, $CaFe_2O_4$ and some Cu-based semiconductors have been developed as photocatalysts for the reduction of water or carbon dioxide [16–23]. However, there is few other p-type oxides photocatalysts reported except for above materials. Take monoclinic $BiVO_4$ for instance, as one of the most promising photocatalysts [7,24–26], there is no report about p-type $BiVO_4$ up to now. This is mainly due to the low formation energy of oxygen vacancy in $BiVO_4$ [27], it is difficult to fabricate p-type $BiVO_4$ for the compensation of oxygen vacancies. Antuch et. al observed an extraordinary photocurrent polarity switching phenomenon in monoclinic $BiVO_4$ [28], but it is simply result from the surface states and the cathodic photocurrent is very weak. As for the $BiVO_4$ with tetragonal scheelite or zircon structure, there are also no corresponding p-type samples reported. To our knowledge, only Xie's group reported a p-type $BiVO_4$ with orthorhombic pucherite structure [29].

On the other hand, the conduction band in the bulk p-type semiconductor is more negative than the surface due to the downward band bending at semiconductor/electrolyte interface. Thus the photo-generate electrons in the bulk have higher energy. In most cases, these photoelectrons relax to the band-edge position in a very short time, ultimately being ejected into the solution at the energy either the conduction band edge or of surface states within the band gap. But according to the study of Nozik et al. [30,31], these photogenerated

* Corresponding author at: School of Material Science and Engineering, University of Jinan, Jinan, 250022, PR China.
** Corresponding authors.
E-mail addresses: mse_wangjp@ujn.edu.cn (J. Wang), mse_yangp@ujn.edu.cn (P. Yang), bbhuang@sdu.edu.cn (B. Huang).

https://doi.org/10.1016/j.apcatb.2019.03.049
Received 21 January 2019; Received in revised form 11 March 2019; Accepted 16 March 2019
Available online 20 March 2019
0926-3373/

electrons are not completely thermalized to the energy of the band edge as they travel through the space charge region in some p-type semiconductors, which is called hot-carrier processes. That is, the electrons reaching the semiconductor surface will carry more energy and have stronger reduction ability. As a result, p-type semiconductor photoelectrode should have stronger reducing power than its n-type counterpart. This phenomenon has been observed in many studies [32–35], however, still not been paid enough attention. If the hot-electron processes are common in p-type semiconductors, water molecules maybe reduced by the p-type semiconductor even its conduction band less negative than the redox potential of H^+/H_2. Again, taking $BiVO_4$ as an example, the conduction band edge of which is located just short of the thermodynamic level for H_2, a little downward bending of the conduction band is helpful to improve the reduction potential of the photogenerate electrons. Therefore, the preparation of p-type $BiVO_4$ is of great significance.

Herein, stable and phase pure p-type tetragonal zircon $BiVO_4$ (P-$BiVO_4$) film was grown on FTO glass via hydrothermal method for the first time. the Mott-Schottky and photoelectrochemical test result indicated that the $BiVO_4$ is a p-type semiconductor. X-ray photoelectron spectroscopy and inductively coupled plasma analysis confirm the existence of Bi vacancies(V_{Bi}) and interstitial oxygen(O_i) in the $BiVO_4$ crystals, density functional theory calculations indicate that the defects lead to a new energy level appearing near the valence band top and the Fermi level shift to the valence band. The onset potential of the photocurrent is about 1.3 V (vs Ag/AgCl), approximately equal to the flat band potential. Combining with diffuse reflection spectrum and X-ray photoelectron spectroscopy, we can figure out that the bottom of the conduction band (CB) of P-$BiVO_4$ located around 0.06 V vs RHE. Though the CB is not negative enough for water reduction to form hydrogen, in consideration of band bending and the hot carriers process, the p-type $BiVO_4$ should posses the hydrogen production capacity in photocatalytic water splitting even without applying any external voltage.

2. Experimental

2.1. Preparation of $BiVO_4$ photoelectrodes

The $BiVO_4$ film grown on FTO glass was prepared by a hydrothermal method. In a typical process, 1 mmol $Bi(NO_3)_3{\cdot}5H_2O$ and 1 mmol ethylenediaminetetraacetic acid disodium were dissolved in 10 ml HNO3 (2 mol L^{-1}) aqueous solution, another 1 mmol NH_4VO_3 and 1 mmol ethylenediaminetetraacetic acid disodium were dissolved in 20 ml NaOH (1 mol L^{-1}) aqueous solution, then the two aqueous were mixed gently and transfer into a 40 ml Teflon-lined autoclave. FTO coated glasses were ultrasonically pretreated respectively in acetone, ethanol and water for 30 min. Then clean FTO glass was put into the Teflon-lined stainless autoclave at an angle against the wall with the conducting side facing down. After the autoclave was sealed, the hydrothermal synthesis was conducted at 160 °C for 12 h. The autoclave was cooled to room temperature naturally and then the FTO glass was taken out and rinsed with deionized water several times and dried at room temperature. The obtained $BiVO_4$ film was named P-$BiVO_4$. To investigate the thermal stability of the P-$BiVO_4$, the P-$BiVO_4$ films were annealed in air at 150 °C, 300 °C, 450 and 600 °C for 1 h, respectively.

Tetragonal zircon $BiVO_4$ powders were prepared by co-precipitation method. 2 mmol $Bi(NO_3)_3{\cdot}5H_2O$ and 2 mmol NH_4VO_3 dissolved in 60 ml distilled water and stirring for 2 h, then the generated yellow precipitate was filtered and washed with distilled water, dried at 100 °C for 5 h, which was named as N-$BiVO_4$.

2.2. Characterization

X-ray diffraction (XRD) patterns were recorded by Bruker D8-Advance X-ray diffractometer with monochromatized Cu Kα radiation (λ = 0.15418 nm). Scanning electron microscopy (SEM) images were recorded on a FEI QUANTA 250 FEG microscope. The high resolution transmission electron microscope (HRTEM) image was recorded on a FEI Tecani F20 microscope.Raman spectroscopy was performed on Horiba LabRAM HR Evolution spectrometer. Inductively Coupled Plasma Optical Emission Spectrometer (ICP-OES) analysis was carried out using an Agilent 5100 ICP-OES (Agilent Technologies, Mulgrave, Australia). X-ray photoelectron spectroscopy (XPS) was recorded on a Thermo Fisher Scientific Escalab 250xi spectrometer. The diffuse reflectance spectra (DRS) was measured using a Hitachi U-4100 spectrometer.

2.3. Electronic structure calculation

DFT calculations were performed in the Vienna ab initio simulation package (VASP). A spin-polarized GGA PBE functional, all-electron plane-wave basis sets with an energy cutoff of 400 eV, and a projector augmented wave (PAW) method were adopted. BiVO4 is simulated using a surface model of p (2 × 2) unit cell periodicity. A (3 × 3 × 1) Monkhorst-Pack mesh was used for the Brillouin-zone integrations to be sampled. Electronic density-of states (DOS) of (4 × 4) supercells were calculated using a higher 9 × 9 × 1 k-point mesh. The conjugate gradient algorithm was used in the optimization. The convergence threshold was set 1*10–4 eV in total energy and 0.05 eV/ Å in force on each atom.

2.4. Photoelectrochemical test

All the (photo)electrochemical measurements were performed in a 0.5 M Na_2SO_4 electrolyte (pH ≈ 6.4) solution using a three-electrode system. The as-prepared films, platinum foil, and Ag/AgCl (3 M KCl) were used as the working electrode, counter electrode, and reference electrode, respectively. Mott-Schottky plots were recorded on Princeton Applied Research EG&G 4000 A potentiostat at frequencies of 5000 Hz and 1000 Hz in the dark. Linear sweep voltammograms were collected on an electrochemical station (CHI660E, China) at a sweep rate of 5 mV/s under chopped light illumination, a 300 W Xe lamp (CEL-HXF300, Beijing CEAU Light, China) was used as light source. All potentials (vs Ag/AgCl) can be converted to RHE (NHE at pH = 0) using the following equation $E_{RHE} = E_{AgCl} + 0.0591\ pH + 0.199\ V$.

2.5. Photocatalytic hydrogen evolution

The photocatalytic hydrogen generation experiment was carried out in a top-irradiation reaction vessel connected to a glass closed gas system (CEL-SPH2N-D9, Beijing CEAU Light, China). P-$BiVO_4$ films were put on the bottom of the Pyrex glass reactor and soak in an aqueous solution (100 mL) containing methanol (20 vol.%) as sacrificial electron donor, 1 wt% Pt was photodeposition on P-$BiVO_4$ as cocatalysts. A 300 W Xe lamp (CEL-HXF300, Beijing CEAU Light, China) was used as light source. The temperature of reaction solution was maintained at 6 °C with cooling water. The generated gases were analyzed by gas chromatography equipped with a thermal conductive detector (TCD).

In order to exclude the influence of the electrode or the external electric field, the P-$BiVO_4$ was scraped from the surface of the FTO (about 6 mg), the P-$BiVO_4$ powders were dispersed in 20 vol% methanol aqueous solution, 1 wt% Pt was photodeposition on P-$BiVO_4$ as cocatalysts. The other condition are the same with above.

2.6. Photoelectrochemical hydrogen evolution

The photoelectrochemical water splitting experiments were carried out in a top-irradiation reaction vessel connected to a glass closed gas system (CEL-SPH2N-D9, Beijing CEAU Light, China). The P-$BiVO_4$ film

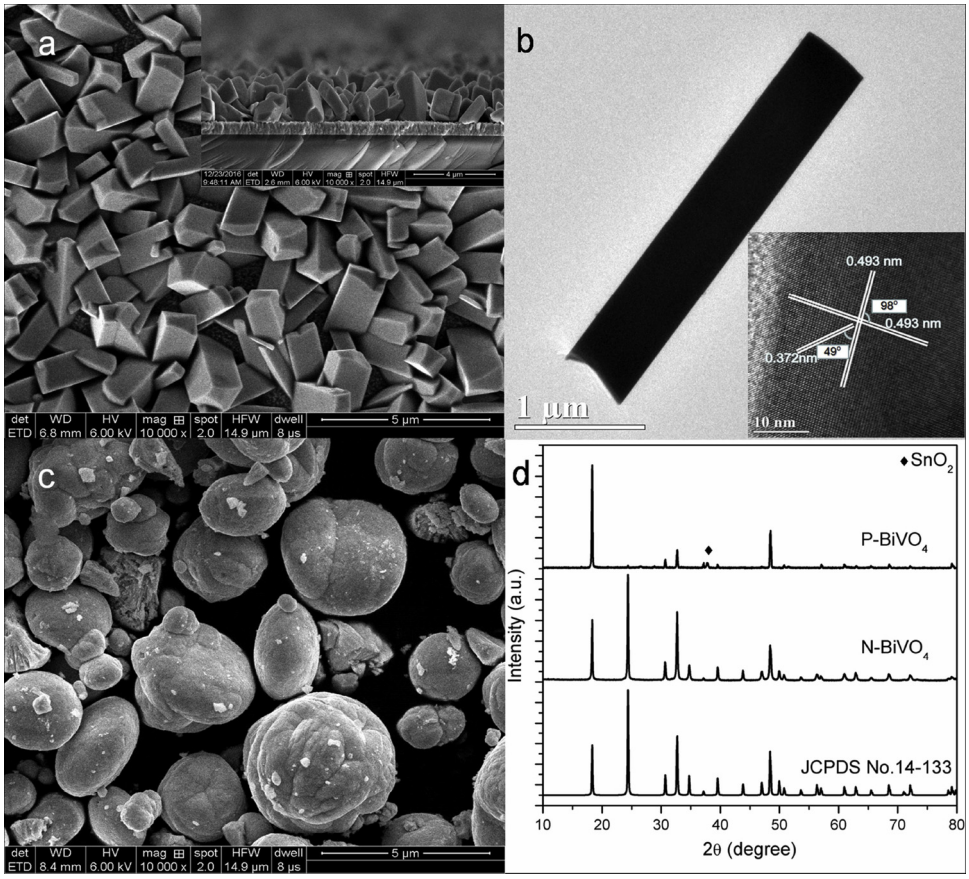

Fig. 1. (a) SEM and (b) TEM images of the P-$BiVO_4$; the inset is the HRTEM image.(c) SEM image of the N-$BiVO_4$ sample. (d) XRD patterns of the $BiVO_4$ samples.

was used as working electrode, Platinum and Ag/AgCl were used as the counter electrode and reference electrode, respectively.

A two-electrode cell was also used to test the hydrogen production activity of P-$BiVO_4$ to exclude the effects of external voltage, in which P-$BiVO_4$ film and Platinum were used as working electrode and counter electrode.

3. Results and discussion

The P-$BiVO_4$ were grown on FTO glass by hydrothermal method. As the scanning electron microscopy (SEM) images show in Figs. 1a and S1a–c, $BiVO_4$ film shows homogeneous morphology within range of vision, all the particles are highly faceted and tetragonal prism structure, with a width about 0.2–1 μm and length about 4 μm, the cross sectional SEM in the inset shows that the thickness of the P-$BiVO_4$ film is about 2 μm. The high resolution transmission electron microscopy (HRTEM) image (Fig. 1b) shows a lattice fringes of 4.93 Å and 3.72 Å, corresponded to the (1 0 1) and (2 0 0) planes of tetragonal zircon structure $BiVO_4$, the surface angles of 49° and 98° are in good agreement with theoretical values of angles between(1 0 1) and (2 0 0) planes. As a contrast, the tetragonal zircon $BiVO_4$ particles (N-$BiVO_4$) prepared by coprecipitation method show irregular spherical shape (shown in Fig. 1c). The X-ray diffraction (XRD) confirmed the tetragonal zircon structure of the as prepared P-$BiVO_4$ film and N-$BiVO_4$ powders. As shown in Fig. 1d, all the diffraction peaks agree well with the tetragonal zircon phase (JCPDS NO. 14-133) and some little impurity phases can be index to SnO_2 (FTO). It is worthwhile to note that the strongest diffraction peak was (101), while the intensity of (200) diffraction peak is very weak, it suggested that the P-$BiVO_4$ prism grown with strong orientation. The structure and uniformity of the film was further ascertained by the Raman spectroscopy which is shown in Fig. S1d, seven vibrational peaks around 855.1 cm^{-1}, 760.26 cm^{-1}, 730.3 cm^{-1}, 366.54 cm^{-1}, 247.50 cm^{-1}, 110.9 cm^{-1}, 62.1 cm^{-1} were found in Raman spectra for P-$BiVO_4$ and N-$BiVO_4$, fixed well with the Raman shift in tetragonal zircon type $BiVO_4$ as reported [36].

The photoelectrochemical properties of the P-$BiVO_4$ film was performed using three-electrode system. The linear-sweep cyclic voltammogram of the P-$BiVO_4$ film electrode under chopped light irradiation is shown in Fig. 2a, a cathodic current was measured when the electrode was illuminated by the light, indicating the p-type conductivity of the P-$BiVO_4$, while the N-$BiVO_4$ show anodic n-type photoresponse in the same potential region. The cathodic current increased with the decreasing of the potential (from 1.5 V to −0.2 V vs Ag/AgCl), and the onset potential of the photocurrent is around 1.3 V (vs Ag/AgCl), which is closed to the flatband potential (E_{fb}) based on the Mott-Schottky analysis shown in Fig. 2b. The negative slope of the Mott-Schottky plots further confirm the p-type conductive properties of the P-$BiVO_4$ film.

Compared with the P-$BiVO_4$ film synthesized by hydrothermal method, the Mott-Schottky plots make clear that the N-$BiVO_4$ shows the character of n-type semiconductor. Normally most of the oxide semiconductors show n-type conductivity for the presence of oxygen vacancies, while the p-type conductivity usually due to the presence of cationic vacancies or interstitial anions in semiconductor [37–40]. In order to find out the reasons for this difference, the Bi and V contents in N-$BiVO_4$ and P-$BiVO_4$ was determined through the ICP analysis. As Table S1 shows, the bismuth element is excessive in N-$BiVO_4$ while insufficient in P-$BiVO_4$. The N-$BiVO_4$ has a higher Bi content, maybe because $Bi(NO_3)_3$ is easier to hydrolyze and precipitate compared with NH_4VO_3 in the process of coprecipitation. The Bi/V ratio is lower than 1 in P-$BiVO_4$, this is due to the high concentration of EDTA complexing a large number of Bi^{3+} ions in the process of hydrothermal reaction, and leads to the loss of Bi in the P-$BiVO_4$ crystal. This implies the existence of Bi vacancies in $BiVO_4$ which can lead to p-type conductivity.

Fig. 3 shows the XP spectra of the Bi 4f, V 2p and O 1s core levels for

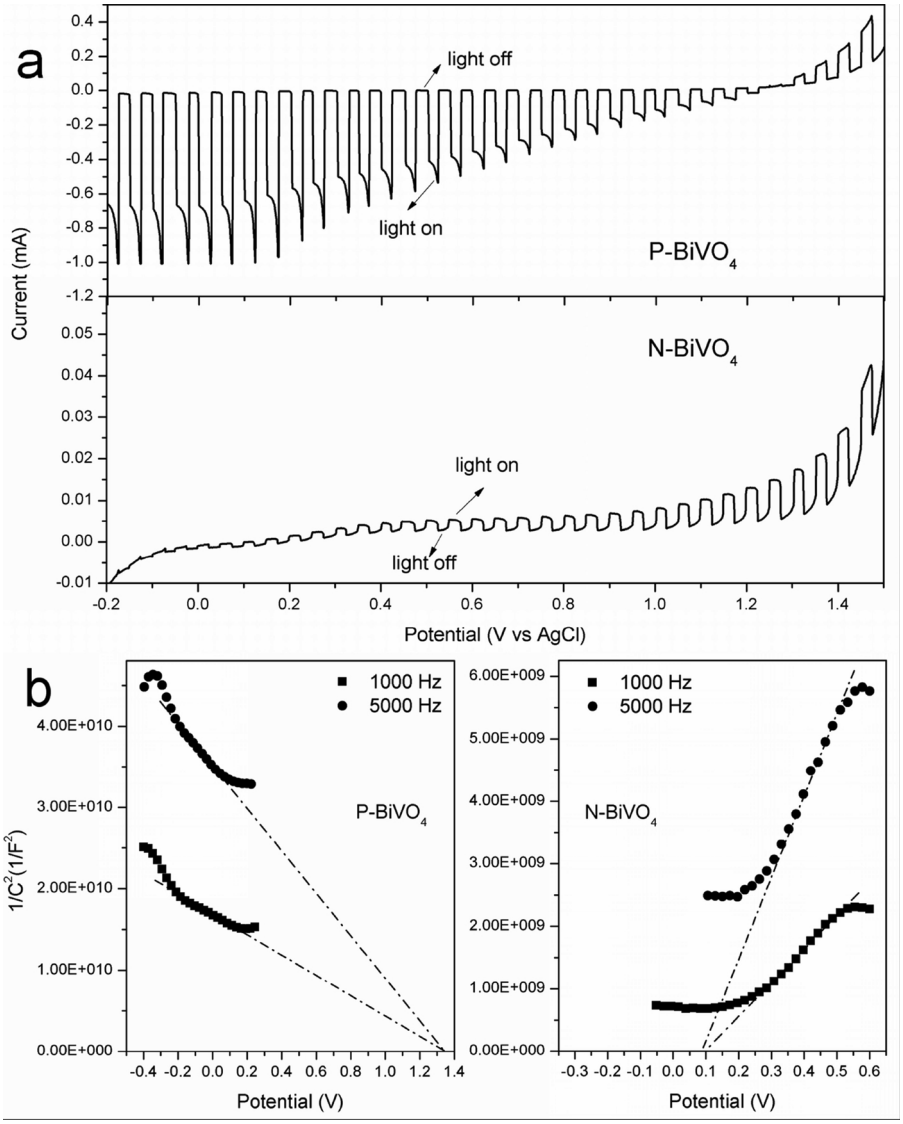

Fig. 2. (a) Linear-sweep cyclic voltammogram of $BiVO_4$ electrodes under chopped light irradiation in an aqueous 0.5 M Na_2SO_4 (pH = 6.4) electrolyte solution. (b) Mott–Schottky plot for the $BiVO_4$ electrodes.

P-$BiVO_4$ film and N-$BiVO_4$ powder. The Bi 4f orbital binding energy of the two materials is almost no difference, as well as V 2p. However, the difference is obvious between the O1 s. The O 1 s peak can be decomposed into three components by Gaussian distribution, which centered at 529.5 eV (O_L), 530.8 eV (O_v) and 532 eV (O_i), respectively. To most oxide compounds, the O_L, O_v, and O_i are usually attributed to the lattice O of $BiVO_4$ crytallites, O^{2-} ions in oxygen-deficient regions and absorbed oxygen species or interstitial oxygen, respectively [41–46]. We

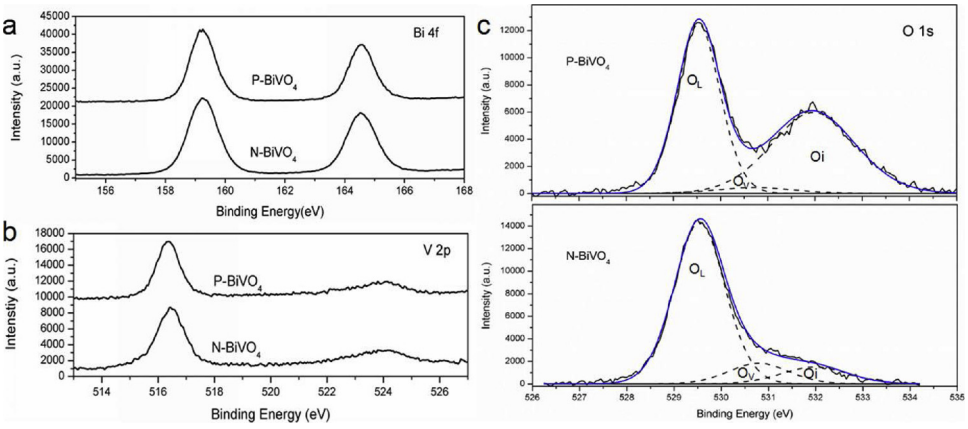

Fig. 3. The Bi4f, V 2p and O1s XP spectra of P-$BiVO_4$ and N-$BiVO_4$ samples.

noticed that the intensity of O_i component of P-$BiVO_4$ film is much stronger than that of N-$BiVO_4$ powder, while the O_v component of P-$BiVO_4$ film is almost negligible. Since it is difficult to adsorb so much oxygen on the surface of the sample, interstitial oxygen could be a major contributor to the O_i peak in P-$BiVO_4$ film [47,48].

Combined with the ICP results, it is easy to create a model to explain the generation of interstitial oxygen. Firstly, Bi vacancies were formed during the growth process due to the strong complexing ability of EDTA. Meanwhile, O vacancies formed in order to balance the charge, in this process, O atom is displaced from its lattice position to an interstitial site, caused the Frenkel defect. Therefore, the Bi vacancies and the interstitial oxygen could be the origin of the p-type conductivity. In order to validate the hypothetical model, DFT calculations are carried out to explore the contribution of each atom to the electronic structures of $BiVO_4$. As shown in Fig. S2, comparing with the defect-free $BiVO_4$, impurity state appears near the top of the valence band when Bi vacancies, oxygen vacancies and interstitial oxygen were introduced into the lattice, and the Fermi level shifts to the valence band. This indicates that the conductivity of $BiVO_4$ change to p-type, and from the analysis of the partial density of states, we find that the impurity energy levels are mainly formed by O elements.

To test the thermal stability of the interstitial oxygen, the P-$BiVO_4$ films were placed at room temperature for 6 months, and annealed at 150 °C, 300 °C, 450 °C, 600 °C for 1 h, respectively. Fig. 4a shows the XRD patterns of P-$BiVO_4$ films after heat treatment at different temperatures, the crystal structure of the P-$BiVO_4$ film change little even after annealing at 450 °C for 1 h, and the $BiVO_4$ transformed to monoclinic phase when the temperature reached 600 °C. SEM images of the samples annealed at different temperatures were shown in Fig. S3. The P-$BiVO_4$ maintains the tetragonal prism structure when the annealing temperature is below 450 °C, but cracks and cavities appear on the surface of P-$BiVO_4$ annealed at 450 °C, and the tetragonal prism structure was completely destroyed when the annealing temperature reached 600 °C. Fig. 4b shows the linear sweep voltammogram of different P-$BiVO_4$ films with chopped illumination. The P-$BiVO_4$ produced cathodic photocurrent at the annealing temperature lower than 450 °C, and the on-set potential decreased with the increased annealing temperature. When the annealing temperature was higher than 450 °C, the P-$BiVO_4$ produced anodic photocurrent. This is in agreement with the results of the Mott Schottky plots shown in Fig. 4c, the flat band potential decreased from 1.3 V to -0.05 V (vs Ag/AgCl) with the rise of temperature, and the P-$BiVO_4$ transforms from p-type conductivity to n-type when the annealing temperature higher than 450 °C. The reasons for this change can be attribute to the decreasing of interstitial oxygen concentration after high temperature treatment. Fig. S4 shows the O 1 s XP spectra of the different BiVO4 samples, compared with origin P-$BiVO_4$, the intensity of O_i peak is almost unchanged when the calcination temperature is lower than 150 °C, and O_i peak decreased while the O_v peak increased with increasing temperature, when the annealing temperature higher than 450 °C, the O_i peak is almost disappear and the O_v become predominant, as the result, the type of conductivity has changed. Based on above results, we can further confirm that interstitial oxygen is the main cause of the p-type conductivity.

XPS valence band spectrum and diffuse reflectance spectroscopy were carried out to clarify the band structure of the $BiVO_4$. From the DRS shown in Fig. S5, we can deduce that the band gap of P-$BiVO_4$ film and N-$BiVO_4$ are 2.85 eV and 2.84 eV, which is consistent with the reported value [18]. Fig. 5a shows the XPS valence band spectrum of P-$BiVO_4$ and N-$BiVO_4$, the valence band position of N-$BiVO_4$ located at 2.1 eV below the Fermi level (E_f), while the valence band edge of N-

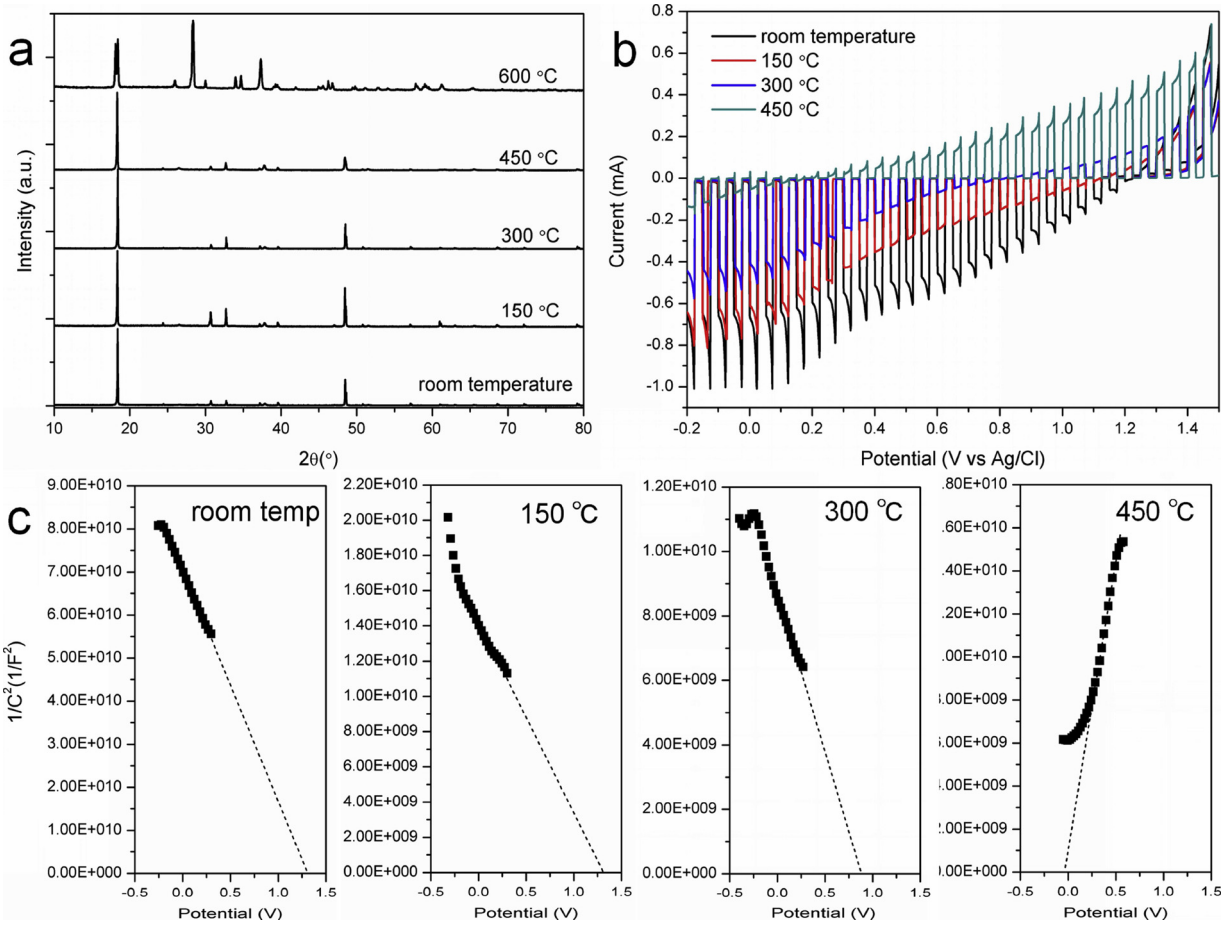

Fig. 4. (a) XRD (b) I–V curves and (c) Mott-Schottky plots of P-$BiVO_4$ annealed at different temperatures.

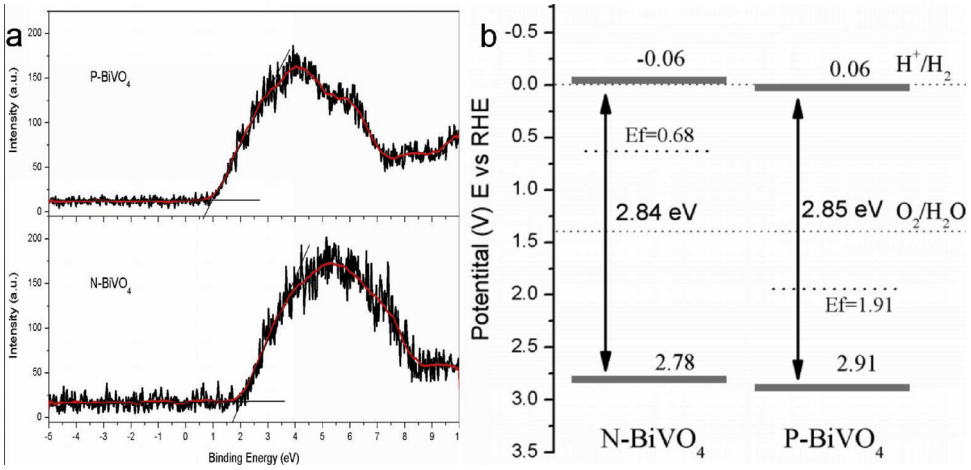

Fig. 5. (a) Valence band edge XPS spectra and (b) Electronic energy-level diagram of the of P-$BiVO_4$ and N-$BiVO_4$.

$BiVO_4$ was observed at 1 eV below the E_f. The position of E_f can be estimated from the Mott-Schottky plots, since E_f is equal to the flat band potential of semiconductors. As shown in Fig. 2b, the flat band potentials of N-$BiVO_4$ powder and P-$BiVO_4$ film were 0.1 V and 1.33 V (vs. Ag/AgCl), respectively. On the basis of these data, the valence band position of P-$BiVO_4$ film and N-$BiVO_4$ powder are calculated to be 2.91 V and 2.78 V (vs RHE), as shown in Fig. 5b, the band structure of both P-$BiVO_4$ and N-$BiVO_4$ are almost the same, the most notable difference is the position of the Fermi level. The conduction band position of P-$BiVO_4$ film and N-$BiVO_4$ powder are 0.06 V and -0.06 V vs. RHE, respectively. It is almost the same as the conduction band position of monoclinic $BiVO_4$, since the conduction bands of both structure are formed by V_{3d} orbits. And this value is consistent with the band structure reported in other studies [18,49]. Taking into account the downward band bending of p-type semiconductor in electrolyte, the P-$BiVO_4$ may possessed the abilities to get hydrogen photogeneration from water under illumination.

The photocatalytic hydrogen generation experiments were carried out to verify the hydrogen production activity of $BiVO_4$. As expected, the N-$BiVO_4$ powder show no hydrogen production activity whether under light or dark condition, while the P-$BiVO_4$ exhibit hydrogen production activity though its conduction band is more positive than N-$BiVO_4$. Fig. 6a shows the time course of H_2 evolution over the P-$BiVO_4$ film under Xe light irradiation. In light condition, the H_2 evolution increases linearly with time, and the H_2 productivity is about 0.25 μmol h^{-1} (active surface area is about 10 cm^2).XRD and SEM images (Fig. S6) shows that, the structure and morphology of the P-BiVO4 were not changed after photocatalytic reaction. In order to exclude the influence of the FTO layer, the P-$BiVO_4$ powder was scraped from the surface of the FTO glass and dispersed in 20 vol% methanol aqueous solution, as shown in Fig. S7, the H_2 productivity is about 0.73 μmol h^{-1} (the weight of scraped P-$BiVO_4$ powder is 6 mg), higher than the P-$BiVO_4$ film, this can be contributed to the larger active surface area compared with the film.

Photoelectrochemical measurements were also performed to investigate the effect of applied potential on hydrogen production efficiency. The photocatalytic H_2 generation experiments of the P-$BiVO_4$ photocathode were carried out at different potential versus Ag/AgCl in 20 vol% methanol aqueous solution. As Fig. 6b shows the hydrogen production rate is about 0.7 μmol h^{-1} at 0 V vs Ag/AgCl, when the potential was fixed at -0.2 V vs Ag/AgCl, the hydrogen production rate reached 3 μmol h^{-1}, is about 4.5 times faster. In order to exclude the influence of the applied electric field, a two-electrode cell consisting of the P-$BiVO_4$ photoelectrode and Pt as the counter electrode was also adopted to verify the hydrogen production activity of $BiVO_4$, the working electrode and counter electrode linked just by a Cu wire, and there is still 1umol H_2 produced after 3.5 h irradiation.

This phenomenon can be attributed to the band bending which caused by built in electrical field at liquid/semiconductor interface. Theoretically, a downward band bending more than 0.06 eV can lift the conduction band of the P-$BiVO_4$ to the position higher than the reduction potential of hydrogen. The band bending is equal to the difference between the Fermi level in the semiconductor and the redox potential of the electrolyte. The Fermi level of P-$BiVO_4$ is located at 1.91 V vs RHE, and it is estimated that the redox potential of the electrolyte is 0.77 V vs RHE through the open circuit potential (OCP) test in dark conditions (Fig. 6c, the Fermi levels of the semiconductor and the redox potential should be equal under equilibrium in dark, $E_f' = E_{f,redox}$). Since the bulit-in electric field will be reduced due to the generation of non-equilibrium carriers under illumination, the Fermi level of P-$BiVO_4$ under illumination (E_f') is aslo estimated by the OCP test. So the band bending ($E_b = E_f' - E_f = qV_b$) is about 1.14 eV in the dark and 0.37 eV under illumination. That is, the conduction band is much higher than 0 V vs RHE whether in the dark or illuminations as Fig. 6d shows. Considering the hot-carrier processes, the H_2 production on P-$BiVO_4$ could be easily understood. The applied potential further aggravates the bending of the band, and the hydrogen production efficiency is also improved. As for the N-$BiVO_4$, whose Fermi level is higher, the conduction band turn more positive and the photo-generate electrons flow from the surface to bulk due to the upward band bending, so there is no hydrogen production under the same condition.

4. Conclusions

In summary, a new p-type tetragonal zircon $BiVO_4$ film was obtained by hydrothermal method. The cathodic photocurrent and negative slope of the Mott-Schottky plots confirm its p-type conductive properties. Though the conduction band is not negative enough for the reduction of water to hydrogen, its p-type conductivity and Built-in Electric Field in depletion layer at liquid/Semiconductor interface make the conduction band shifted to a more negative potential, and the hot-electron process make the P-$BiVO_4$ exhibit hydrogen production activity while illuminated even without any external voltage. Thus, the p-type tetragonal zircon $BiVO_4$ is a promising candidates for photocathode material in PEC applications. More importantly, this reveals the important role of hot electron process in photoreduction reaction. It remind us that the same kind of semiconductor can have stronger photo-reduction ability, just by changing its conduction type.

Acknowledgments

This work was supported by the National Natural Science

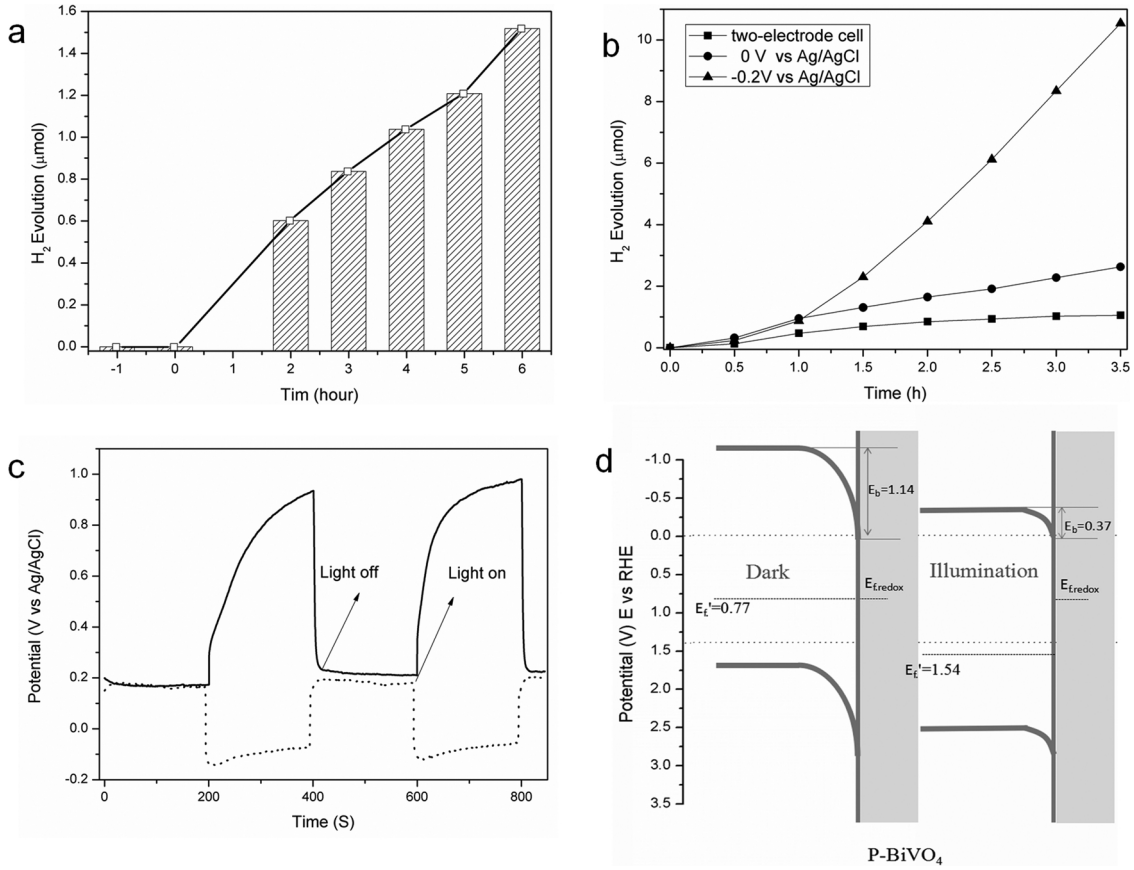

Fig. 6. (a) The photocatalytic and (b) Photoelectrochemical hydrogen evolution under 300 W Xe lamp irradiation for P-$BiVO_4$ film.. (c) Open Circuit Potential of P-$BiVO_4$ under dark and illumination (black line), the red line is the OCP of P-$BiVO_4$ after 450 °C annealing. (d) The band bending of P-$BiVO_4$ in the dark and illumination conditions (For interpretation of the references to colour in this figure legend, the reader is referred to the web version of this article).

Foundation of China (51402124, 51402123 and 51602128), Natural Science Foundation of Shandong Province (No. BS2014CL020), and China Postdoctoral Science Foundation (No. 2016M590610).

Appendix A. Supplementary material

Supplementary data associated with this article can be found in the online version at doi:

Appendix B. Supplementary data

Supplementary material related to this article can be found, in the online version, at doi:https://doi.org/10.1016/j.apcatb.2019.03.049.

References

[1] J. Tian, N. Cheng, Q. Liu, W. Xing, X. Sun, Angew. Chem. Int. Ed. 54 (2015) 5493–5497.
[2] I. Dincer, Int. J. Hydrogen Energy 37 (2012) 1954–1971.
[3] J. Tian, Q. Liu, A.M. Asiri, X. Sun, J. Am. Chem. Soc. 136 (2014) 7587–7590.
[4] T. Liu, K. Wang, G. Du, A.M. Asiri, X. Sun, J. Mater. Chem. A 4 (2016) 13053–13057.
[5] S.U. Khan, M. Al-Shahry, W.B. Ingler, Science 297 (2002) 2243–2245.
[6] X. Yang, A. Wolcott, G. Wang, A. Sobo, R.C. Fitzmorris, Q. Fang, J. Zhang, Y. Li, Nano Lett. 9 (2009) 2331–2336.
[7] T.W. Kim, K.S. Choi, Science 343 (2014) 990–994.
[8] D.K. Zhong, D.R. Gamelin, J. Am. Chem. Soc. 132 (2010) 4202–4207.
[9] J.F. Guayaquil-Sosa, B. Serrano Rosales, P.J. Valadés-Pelayo, S. Escobedo, H. de Lasa, Appl. Catal. B 211 (2017) 337–348.
[10] C. Bojer, J. Schöbel, T. Martin, M. Ertl, H. Schmalz, J. Breu, Appl. Catal. B: Environ. 204 (2017) 561–565.
[11] B. Zhang, H. Zhang, Z. Wang, X. Zhang, X. Qin, Y. Dai, Y. Liu, P. Wang, Y. Li, B. Huang, Appl. Catal. B: Environ. 211 (2017) 258–265.
[12] M.-W. Kim, H. Yoon, T.Y. Ohm, H.S. Jo, S. An, S.K. Choi, H. Park, S.S. Al-Deyab, B.K. Min, M.T. Swihart, Appl. Catal. B: Environ. 201 (2017) 479–485.
[13] A.Y. Ahmed, M.G. Ahmed, T.A. Kandiel, Appl. Catal. B: Environ. 236 (2018) 117–124.
[14] P. Ágoston, K. Albe, R.M. Nieminen, M.J. Puska, Phys. Rev. Lett. 103 (2009) 245501.
[15] A.J. Nozik, R. Memming, J. Phys. Chem. 100 (1996) 13061–13078.
[16] S. Wang, L. Pan, J.J. Song, W. Mi, J.J. Zou, L. Wang, X. Zhang, J. Am. Chem. Soc. 137 (2015) 2975–2983.
[17] Y. Lin, Y. Xu, M.T. Mayer, Z.I. Simpson, G. McMahon, S. Zhou, D. Wang, J. Am. Chem. Soc. 134 (2012) 5508–5511.
[18] S. Ida, K. Yamada, T. Matsunaga, H. Hagiwara, Y. Matsumoto, T. Ishihara, J. Am. Chem. Soc. 132 (2010) 17343–17345.
[19] U.A. Joshi, P.A. Maggard, J. Phys. Chem. Lett. 3 (2012) 1577–1581.
[20] L. Fuoco, U.A. Joshi, P.A. Maggard, J. Phys. Chem. C 116 (2012) 10490–10497.
[21] J. Gu, Y. Yan, J.W. Krizan, Q.D. Gibson, Z.M. Detweiler, R.J. Cava, A.B. Bocarsly, J. Am. Chem. Soc. 136 (2014) 830–833.
[22] Z. Wei, J.S. Hu, K.J. Zhu, W.Q. Wei, X.G. Ma, Y.F. Zhu, Appl. Catal. B: Environ. 226 (2018) 616–623.
[23] T. Wang, Y. Wei, X. Chang, C. Li, A. Li, S. Liu, J. Zhang, J. Gong, Appl. Catal. B: Environ. 226 (2018) 31–37.
[24] A. Kudo, K. Ueda, H. Kato, I. Mikami, Catal. Lett. 53 (1998) 229–230.
[25] A. Kudo, K. Omori, H. Kato, J. Am. Chem. Soc. 121 (1999) 11459–11467.
[26] Y. Park, K.J. McDonald, K.S. Choi, Chem. Soc. Rev. 42 (2013) 2321–2337.
[27] W. Yin, S.H. Wei, M.M. Al-Jassim, J. Turner, Y. Yan, Phys. Rev. B 83 (2011) 155102.
[28] M. Antuch, P. Millet, A. Iwase, A. Kudo, Appl. Catal. B: Environ. 237 (2018) 401–408.
[29] S. Gao, B.C. Gu, X.C. Jiao, Y.F. Sun, X.L. Zu, F. Yang, W.G. Zhu, C.M. Wang, Z.M. Feng, B.J. Ye, Y. Xie, J. Am. Chem. Soc. 139 (2017) 3438–3445.
[30] J.A. Turner, A.J. Nozik, Appl. Phys. Lett. 41 (1982) 101–103.
[31] C.A. Koval, P.R. Segar, J. Am. Chem. Soc. 111 (1989) 2004–2010.
[32] J.R. McKone, A.P. Pieterick, H.B. Gray, N.S. Lewis, J. Am. Chem. Soc. 35 (2012) 223–231.
[33] A.J. Bard, A.B. Bocarsly, F.R.F. Fan, E.G. Walton, M.S. Wrighton, J. Am. Chem. Soc. 102 (1980) 3671–3677.
[34] A. Heller, R.G. Vadimsky, Phys. Rev. Lett. 46 (1981) 1153.
[35] J.A. Baglio, G.S. Calabrese, D.J. Harrison, E. Kamieniecki, A.J. Ricco, M.S. Wrighton, G.D. Zoski, J. Am. Chem. Soc. 105 (1983) 2246–2256.
[36] R.L. Frost, D.A. Henry, M.L. Weier, W. Martens, J. Raman Spectrosc. 37 (2006) 722–732.

[37] S. Lany, A. Zunger, Phys. Rev. Lett. 98 (2007) 045501.
[38] H. Raebiger, S. Lany, A. Zunger, Phys. Rev. B 76 (2007) 045209.
[39] A. Zunger, Appl. Phys. Lett. 83 (2003) 57–59.
[40] Z. Wang, P.K. Nayak, J.A. Caraveo－Frescas, H.N. Alshareef, Adv. Mater. 28 (2016) 3831–3892.
[41] U. Ilyas, R.S. Rawat, T.L. Tan, P. Lee, R. Chen, H.D. Sun, F. Li, S. Zhang, J. Appl. Phys. 110 (2011) 093522.
[42] A. Sahai, N. Goswami, Ceram. Int. 40 (2014) 14569–14578.
[43] K.H. Tam, C.K. Cheung, Y.H. Leung, A.B. Djuriš´ić´, C.C. Ling, C.D. Beling, S. Fung, W.M. Kwok, W.K. Chan, D.L. Phillips, L. Ding, W.K. Ge, J. Phys. Chem. B 110 (2006) 20865–20871.
[44] Y.J. Jeong, T.K. An, D.J. Yun, L.H. Kim, S. Park, Y. Kim, S. Nam, K.H. Lee, S.H. Kim, J. Jang, C.E. Park, ACS Appl. Mater. Interfaces 8 (2016) 5499–5508.
[45] J.C. Fan, J.B. Goodenough, J. Appl. Phys. 48 (1977) 3524–3531.
[46] Y.F. Hsu, Y.Y. Xi, K.H. Tam, A.B. Djurisic, J. Luo, C.C. Ling, C.K. Cheung, A.M.C. Ng, W.K. Chan, X. Deng, C.D. Beling, S. Fung, K.W. Cheah, P.W.K. Fong, C.C. Surya, Adv. Funct. Mater. 18 (2008) 1020–1030.
[47] S.T. Tan, X.W. Sun, Z.G. Yu, P. Wu, G.Q. Lo, D.L. Kwong, Appl. Phys. Lett. 91 (2007) 072101.
[48] H. Kawazoe, M. Yasukawa, H. Hyodo, M. Kurita, H. Yanagi, H. Hosono, Nature 389 (1997) 939.
[49] R. Chen, W. Wang, D. Jiang, X. Chu, X. Ma, Q. Zhan, J. Phys. Chem. Solids 117 (2018) 28–35.